
# Mineralized Collagen Fibril Network Spatial Arrangement Influences Cortical Bone Fracture Behavior

Yaohui Wang, Ani Ural

PII: S0021-9290(17)30578-X
DOI: https://doi.org/10.1016/j.jbiomech.2017.10.038
Reference: BM 8440

To appear in: *Journal of Biomechanics*

Accepted Date: 28 October 2017

Please cite this article as: Y. Wang, A. Ural, Mineralized Collagen Fibril Network Spatial Arrangement Influences Cortical Bone Fracture Behavior, *Journal of Biomechanics* (2017), doi: https://doi.org/10.1016/j.jbiomech.2017.10.038

# MINERALIZED COLLAGEN FIBRIL NETWORK SPATIAL ARRANGEMENT INFLUENCES CORTICAL BONE FRACTURE BEHAVIOR

Yaohui Wang[1], Ani Ural[1]

[1]Department of Mechanical Engineering, Villanova University,
800 Lancaster Avenue, Villanova, PA

**Full Length Article**

Word count: 4059

**Corresponding Author**

Ani Ural

Associate Professor

Department of Mechanical Engineering

Villanova University

800 Lancaster Avenue, Villanova, PA 19085

E-mail: ani.ural@villanova.edu

Phone:(610) 519-7735

Fax: (610) 519-7312

**ABSTRACT**

Bone is a hierarchical material exhibiting different fracture mechanisms at each length scale. At the submicroscale, the bone is composed of mineralized collagen fibrils (MCF). At this scale, the fracture processes in cortical bone have not been extensively studied in the literature. In this study, the influence of MCF size and orientation on the fracture behavior of bone under both transverse and longitudinal loading was investigated using novel 3D models of MCF networks with explicit representation of extra-fibrillar matrix. The simulation results showed that separation between MCFs was the main cause of damage and failure under transverse loading whereas under longitudinal loading, the main damage and failure mechanism was MCF rupture. When the MCF network was loaded in the transverse direction the mechanical properties increased as the orientation of fibrils deviated farther from the main fibril orientation whereas the opposite trend was observed under longitudinal loading. The fracture energy was much larger in longitudinal than transverse loading. MCF diameter variation did not affect the mechanical properties under longitudinal loading but led to higher mechanical properties with increasing MCF diameter under transverse loading. The new modeling framework established in this study generate unique information on the effect of MCF network spatial arrangement on the fracture behavior of bone at the submicroscale which is not currently possible to measure via experiments. This unique information may improve the understanding of how structural alterations at the submicroscale due to disease, age-related changes, and treatments affect the fracture processes at larger length scales.

***Keywords:*** *Mineralized collagen fibril*; *extra-fibrillar matrix*; *cortical bone; cohesive finite element modeling; submicroscale*

## 1. INTRODUCTION

Bone is a hierarchically structured composite material which exhibits different fracture mechanisms at each length scale spanning nano- to macroscale. The basic components of bone, collagen and mineral, form mineralized collagen fibrils (MCF) which then arrange into fibril arrays at the submicroscale.

MCFs have been hypothesized to contribute to the fracture toughness of bone by bridging cracks (Nalla et al., 2003) or by delamination of the fibrils from one of the crack surfaces which activate the separation of the extra-fibrillar matrix between fibrils (Fantner et al., 2006). The separation of extra-fibrillar matrix between MCFs has been postulated as a significant energy dissipation mechanism preceding the formation of microcracks (Fantner et al., 2005). Other experimental studies have reported interfibrillar sliding as a protective mechanism against fracture (Gupta et al., 2006; Zimmermann et al., 2011). Although, these studies have identified the important mechanisms through which MCF networks contribute to the fracture resistance of bone, the amount of contribution of these factors to fracture toughness at larger length scales is still not well understood, particularly, due to the challenges of experimental evaluation at this scale. Furthermore, the contribution of spatial arrangement and size of MCFs to fracture toughness has not been evaluated even though MCF orientation (Fratzl et al., 2004;

Jimenez-Palomar et al., 2015; Martin and Ishida, 1989; Peterlik et al., 2006; Ramasamy and Akkus, 2007) and diameter (Parry et al., 1978) have been observed to influence the mechanical properties of bone.

There are quite a few computational models that have analyzed the mechanical behavior of a single MCF as in (Buehler, 2007; Hambli and Barkaoui, 2012; Luo et al., 2011; Nair et al., 2013; Siegmund et al., 2008). However, the number of computational studies that evaluated the mechanical behavior of MCF arrays is limited. One of these studies generated a quasi-planar spatially random MCF network represented as line elements with perfect bonding and evaluated the elastic properties of the MCF network as a function of volume fraction (Jasiuk and Ostoja-Starzewski, 2004). A 2D regular array of MCFs and noncollagenous proteins separated by an interface was developed to evaluate the stress-strain response of MCF arrays (Hamed and Jasiuk, 2013). Another 2D study simulated three-point bending of a regular staggered array of MCFs and investigated the effect of MCF fibril length, thickness, and failure energy of the protein matrix on the maximum force and area under the load displacement curve (Lai and Yan, 2017). A very recent study evaluated the cyclic behavior of 2D regular staggered arrays of MCFs utilizing stiffness degradation of the interfibrillar interface (De Falco et al., 2016b).

The computational models summarized above did not capture the complex 3D structure of MCF networks that exhibit plywood structure, varying orientation angles, and merging of fibrils. In addition, they did not quantify the fracture properties of the bone. As a result, to address these gaps, in this study we develop a novel approach for modeling 3D MCF networks to evaluate their mechanical response including damage and fracture behavior. The models evaluate both the breaking and separation of fibrils through different modes of loading and provide unique information on the effect of MCF network spatial arrangement on the fracture behavior of bone at the submicroscale which is not currently possible to measure via experiments. Understanding the influence of MCF network properties on fracture may help better understand how the alterations at this scale due to disease, age-related changes, and treatments affect the fracture processes at larger length scales.

## 2. METHODS

Finite element models of MCF unit cells were utilized to evaluate the influence of MCF network orientation and size on the cortical bone fracture response under tensile loading in two different directions representing rupture and delamination (separation of extra-fibrillar matrix) of MCFs. The details of the modeling approach are described in the subsequent sections.

## 2.1 Finite Element Model Generation

### *2.1.1 MCF Network Model Generation*

The detailed models of MCF networks were generated by a newly developed MATLAB (MathWorks, Natick, MA) script in conjunction with the finite element software, ABAQUS (version 6.14, Simulia, Providence, RI). The generation of the MCF network models consisted of the following steps:

(1) In the MATLAB script, the location of two endpoints and diameter of each fibril was generated one at a time within the desired orientation and diameter range. Each individual MCF was idealized as a straight cylinder with a constant diameter. The first endpoint of the fibril was generated randomly followed by the calculation of the orientation angle according to the plywood structure rotation rate. Then, the coordinates of the second endpoint was calculated based on the orientation angle and a random dispersion angle.

(2) The distances between the new fibril and existing fibrils were calculated to perform an overlapping check to determine whether to keep the latest generated fibril. In order to represent the penetration of MCFs in real bone (Wallace et al., 2010), while maintaining their cylindrical-like shape, an overlap criteria that allowed for a maximum cut depth of 35% of a MCF's diameter was utilized.

(3) Once sufficient number of fibrils were generated corresponding to the desired volume fraction, the MCFs were separated into two groups according to the fibrils' length: long MCFs (that run through the whole model), and short MCFs (at least one end is within the model domain with a minimum length of 0.4 μm) (Fig. 1a, b).

(4) Long and short MCFs were again separated into groups within which the fibrils were not overlapped with each other (Fig. 1c). For most models, five groups (three groups for long fibrils, two for short fibrils) were enough to separate the overlapping fibrils. The separation process enabled the model to avoid irregular interface surfaces after the trimming process.

(5) The MCF groups generated in MATLAB were transferred to ABAQUS using a newly developed Python script. The overlapped regions between MCFs were trimmed by utilizing the groups formed in Step (4) so that as many long fibrils have uncut cylindrical shapes (Fig. 1d). The parts of the MCFs extending outside of the unit cell volume were also trimmed.

(6) The trimmed MCFs were assembled to generate the complete model geometry (Fig. 1e) and were meshed using tetrahedral elements.

(7) A layer of zero thickness cohesive elements were added to the outer surfaces of the fibrils to represent the extra-fibrillar matrix as an interface between the MCFs. MCFs were defined as enriched crack regions (Section 2.2).

(8) Boundary conditions (Section 2.1.2) and material properties (Section 2.1.3) were assigned to all models to complete the model generation.

*2.1.2 Boundary Conditions and Loading*

The models were evaluated under tensile transverse (perpendicular to the main MCF direction) and longitudinal (parallel to the main MCF direction) displacement loading (Fig. 2) representing the energy dissipation due to the separation of extra-fibrillar matrix and the rupture of fibrils bridging microcracks, respectively. The models were fixed directly opposite to the loading face and symmetric boundary conditions were applied to the two mutually perpendicular

faces to assure that the free surfaces have the same transverse displacement at any point on the surface (Fig. 2). Symmetric boundary conditions were chosen due to the negligible difference between the results obtained using periodic and symmetric boundary conditions (Hbaieb et al., 2007).

*2.1.3 Material Properties*

The models incorporated two phases including the MCFs and the extra-fibrillar matrix represented as interfaces between the MCFs. The MCF elastic modulus was selected based on the mean value reported in tensile testing of individual MCFs (Hang and Barber, 2011) (Table 1). There is no reported Poisson's ratio in the literature for MCFs, therefore, it was chosen based on typical values used in modeling of MCFs (Hambli and Barkaoui, 2012). The elastic properties of the extra-fibrillar matrix is not required as it is represented as a cohesive interface.

The properties required for the cohesive models (Section 2.2) are the ultimate strength, and critical energy release rate for both MCFs and the extra-fibrillar matrix. Fracture properties for the extra-fibrillar matrix were adopted from fibril pull-out tests performed on individual MCFs which provided the interfacial shear strength and fracture energy (Hang et al., 2014) (Table 1). An adjustment factor was applied to the shear strength and fracture energy to account for the representation of the extra-fibrillar matrix as an interface in the models which resulted in a smaller effective interfacial surface area. This adjustment factor (1.5) was calculated based on single fibril pull-out simulations performed to match the experimental results. Since there is no normal strength reported in the literature for the extra-fibrillar matrix, it was assumed to be twice that of the shear strength based on typical ratios for other materials including bone.

The ultimate strength of the MCFs were adopted from tensile tests performed on individual MCFs in which MCFs demonstrated instantaneous failure (Hang and Barber, 2011). In order to reproduce this behavior, the separation distance leading to MCF failure was chosen as two orders of magnitude lower than the extra-fibrillar matrix while ensuring numerical convergence. This allowed for calculation of the fracture energy (Table 1) based on the bilinear cohesive model (Section 2.2).

**2.2. Fracture Modeling via Traction-Separation Cohesive Models**

Fracture behavior was represented by a traction-separation cohesive model (Fig. 3). The cohesive behavior was implemented in the MCFs via the extended finite element method (XFEM). The XFEM enriched regions in MCFs accounted for fibril rupture. The separation of the extra-fibrillar matrix between MCFs was represented by interface elements. In both approaches, the cohesive model was defined by the ultimate strength and critical energy release rate. In this study, a linear damage evolution curve (Fig. 3) was selected based on previous simulations on bone that showed agreement with experimental data (Ural and Vashishth, 2006). Damage initiation was represented by a quadratic equation $(T_n/\sigma_{nc})^2 + (T_s/\sigma_{sc})^2 + (T_t/\sigma_{tc})^2 = 1$, where $T_n$, $T_s$ and $T_t$ are the current stress values in normal and shear directions and $\sigma_{nc}$, $\sigma_{sc}$ and $\sigma_{tc}$ are ultimate normal and shear strengths. For damage initiation, the values for shear in both directions were assumed to be the same ($\sigma_{sc} = \sigma_{tc}$). Damage evolution is defined by an effective critical energy release rate, $G_c$, that represents the coupled normal and shear fracture energy. The details of cohesive modeling in bone is provided in (Ural and Vashishth, 2006).

### 2.3 Finite Element Models Generated and Simulations Run

A total of nine distinct models of MCF networks were built to investigate the influence of diameter and orientation on the mechanical response of bone at the submicroscale. The packing structure of MCFs in the model unit cell while maintaining a consistent distribution of fibril length resulted in an upper bound in the volume fraction between 72-75% depending on the MCF orientation which is in line with the reported values in the literature (Fritsch et al., 2009).

Three different diameter values were investigated including 60±5 nm, 80±5nm, 100±5nm based on the range of values reported in the literature (Bätge et al., 1997; Tzaphlidou, 2005, 2008). The diameter deviation range of 10 nm (±5 nm) was incorporated to more realistically represent the variance in the MCF size in bone. In these models, the volume fraction was kept constant at 75%. The orientation of the fibrils were predominantly parallel with a dispersion value of ±15° in all planes with respect to the main fibril direction based on experimental measurements (Reznikov et al., 2013).

In order to assess the influence of orientation, the volume fraction and the diameter of the MCFs were kept constant at 72% and 100±5nm, respectively, and only the orientation of the MCFs were varied. A diameter value of 100 nm was chosen for these analysis as it is closer to the value reported for human bone (Reznikov et al., 2013). Six models were generated with a plywood pattern incorporating a rotation rate of 30°, 60°, 90° resulting in MCF fibril orientations of 0°/30°, 0°/60°, 0°/90°, ±15°, ±30°, ±45° with a xy-plane (Fig. 2) dispersion of ±15° based on the literature (Reznikov et al., 2013).

Finite element meshes of the models consisted of 1.6-2.2 million tetrahedral elements and

200,000-250,000 cohesive interface elements. This mesh size was determined based on a mesh convergence study. The number of fibrils ranged from 200 to 700 in the models incorporating diameter variation, and was about 250 for models with orientation variation. The simulations were run using a parallel computing system with 48 cores.

### 2.4. Analysis of Results

The simulation results were processed to evaluate the elastic modulus, ultimate strength and fracture energy of each model. The elastic modulus and ultimate strengths were extracted from the stress-strain curve that was obtained from the load-displacement response of each model. In addition, the mode of damage and failure was evaluated for each simulation by observing if there is separation or rupture of fibrils.

The fracture energy was calculated as the total energy that was associated with damage and crack formation at the cohesive interface elements and in enriched XFEM regions. Under transverse loading, the extra-fibrillar matrix do not completely separate due to the large deformation required for full separation comparable to the size of the unit cell. Therefore, in transverse models, the fracture energy was evaluated at 30% strain corresponding to the stage when a clear crack surface was formed. On the other hand, under longitudinal loading, the fracture energy was calculated at ~5% strain corresponding to the ultimate strength as the stress dropped rapidly after that point.

## 3. RESULTS

Finite element simulations on each model under two loading conditions were run and the results were analyzed. The results showed that the MCF networks had much larger elastic

modulus, ultimate strength and fracture energy under longitudinal loading compared to transverse but they achieved larger ultimate strain under transverse loading (Fig. 5, 6, Table 2). Separation between MCFs was the main cause of damage and failure under transverse loading (Fig. 4). Under longitudinal loading, the main damage and failure mechanism was breaking of MCFs and the separation of MCFs was a minor contributor (Fig. 4).

MCF diameter variation did not affect the elastic modulus, ultimate strength and fracture energy under longitudinal loading as similar to a typical fiber reinforced composite (Fig. 5a, Table 2). Under transverse loading, increasing fibril diameter led to higher elastic modulus, ultimate strength, and fracture energy (Fig. 5b, Table 2).

The variation in the MCF orientation led to different behavior under longitudinal and transverse loading. When the MCF network was loaded in the transverse direction the elastic modulus, ultimate strength and fracture energy increased as the orientation of fibrils deviated farther from the main fibril orientation whereas the opposite trend was observed under longitudinal loading. (Fig. 6, Table 2). The fracture energy was much larger in longitudinal than transverse loading (Table 2) even at much lower strains.

## 4. DISCUSSION

This study investigated the influence of MCF fibril size and orientation on the fracture behavior of bone at the submicroscale under both transverse and longitudinal loading using novel 3D models of MCF networks. The newly developed modeling approach for MCF networks allowed for a more realistic 3D representation of the bone at the submicroscale and explicitly incorporated the extra-fibrillar matrix. The simulation results showed that the MCF spatial

arrangement and size influence the fracture behavior. The damage mode of the MCF network (i.e. fibril rupture or separation) also played a significant role in contributing to fracture behavior.

The simulations under transverse and longitudinal loading activated the fibril separation and rupture mechanisms, respectively, as observed in experiments (Fantner et al., 2005; Nalla et al., 2003). The fibril rupture occurred at a smaller deformation but required more energy, whereas fibril separation was associated with a very large deformation but needed less energy. These findings indicate that crack bridging via MCFs can play an important role in fracture resistance due to the energy required to break the fibrils. Previous studies also identified fibril sliding as a mechanism of energy dissipation under longitudinal loading (Gupta et al., 2006; Zimmermann et al., 2011). In the simulations, fibrillar sliding prior to fibril rupture was predominantly observed between long and short MCFs and composed about 10% of the fracture energy at the MCF rupture point. Although fibril separation initiated and proceeded at a much lower load level and was associated with a lower energy dissipation compared to fibril rupture, extensive deformation (several microns) compared to the MCF size is required for attaining complete fibril separation. Therefore, the stress transfer between the MCFs via the extrafibrillar matrix would still exist until this full separation is attained and provide resistance to full microcrack formation. This process may act as an effective mechanism of energy dissipation and protect against full microcrack formation at larger length scales. Furthermore, even under longitudinal loading, extra-fibrillar matrix may contribute to the resistance to microcrack formation as it can continue to hold the ruptured MCFs together due to its capability to accommodate much larger deformation.

The MCF orientation played a significant role in determining the mechanical response of bone at the submicroscale. Under transverse loading, as the MCFs deviated farther from the main fibril direction, all mechanical properties (elastic modulus, ultimate strength, and fracture energy) increased. This is due to the fact that MCFs were no longer parallel to the loading direction with increasing orientation angle. As a result, the resistance was not only due to extra-fibrillar matrix separation but also due to MCFs. Under longitudinal loading, the opposite behavior was observed. As the MCFs deviated farther from the main fibril and loading direction, more extra-fibrillar matrix was exposed to separation reducing all the mechanical properties. These results indicate that loading direction with respect to the MCF orientation is a significant determinant of resistance to crack growth which is in line with experimental observations (Peterlik et al., 2006). At the next length scale, the variation of MCF orientation in different regions of the lamellae and from one layer to another may provide an effective mechanism to prevent crack growth as a wide range of MCF orientations activate different resistance mechanisms.

The MCF diameter only affected the mechanical properties under transverse but not longitudinal loading. Reduction in MCF diameter led to an increase in interface area (i.e. the extra-fibrillar matrix) between the MCFs. Therefore, under transverse loading, the larger area of extra-fibrillar matrix resulted in a reduction in all mechanical properties. On the other hand, under longitudinal loading, due to the small contribution of extra-fibrillar matrix to the mechanical response when the MCFs are almost aligned with the loading, the mechanical response was very similar in all MCF diameters.

The elastic properties of the MCF network reported in this study were lower compared to the elastic modulus of bone at larger length scales. This is due to the low MCF elastic modulus adopted in the simulations based on experimental measurements (Hang and Barber, 2011) as well as continuum and molecular dynamics simulations (Buehler, 2007; Hambli and Barkaoui, 2012; Nair et al., 2013) on an individual MCF. This difference is most likely due to the more complex structure attained at larger length scales in bone improving the mechanical properties compared to the properties at lower length scales. On the other hand, the ultimate strength of MCF networks under longitudinal loading was in the range of values measured parallel to the osteons (Reilly and Burstein, 1975). The comparable values are due to the ultimate strength of a single MCF that is in the same order of magnitude as the bone. As expected, the mechanical properties under transverse loading were even lower as they depend on the properties of the extra-fibrillar matrix which is predominantly composed of noncollagenous proteins. It should be noted that this study does not directly predict the response of bone at larger length scales because there are other structural features that significantly contribute to mechanical behavior at micro- to macroscale. The results represent the local material properties within a single lamella and capture the mechanical response at the submicroscale. These results can also serve as inputs into the models of lamellae at the next length scale as a part of a multiscale modeling framework for evaluating the mechanical behavior of bone.

The findings of this study can provide insights into the modifications in material response at the submicroscale due to osteoporosis. Although there is limited data on the structural changes that occur in MCF networks due to osteoporosis, reduction in diameter as well as a more random

orientation of MCFs was reported in osteoporotic rat bones compared to normal ones (Kafantari et al., 2000). Our results showed that the reduction in diameter did not influence the response under longitudinal loading (fibril rupture) but had an adverse effect on the response under transverse loading (separation of fibrils). This may indicate a reduced energy dissipation mechanism in fibril separation due to osteoporosis compared to normal bone based on structural changes at the submicroscale. The highest volume fraction that can be achieved in our models with random orientation of fibrils within the same volume was lower than the organized MCF orientations presented in this study. This reduced volume fraction is expected to lead to a reduction in all material properties and may highlight the additional adverse influence of structural changes at the submicroscale in osteoporotic bone.

The main strength and novelty of this study is the three-dimensional representation of MCF networks. The limited number of studies on MCF networks utilized 2D, parallel and uniformly arranged MCFs (De Falco et al., 2016a; Lai and Yan, 2017) and were not able to capture the orientation variation in MCFs that is observed at the submicroscale. Only one quasi-planar study (Jasiuk and Ostoja-Starzewski, 2004) investigated two different in-plane orientations without extrafibrillar matrix and found only variation in transverse elastic properties with the change in orientation. The elastic modulus values found in that study were larger than the current study due to the high elastic modulus assigned to single MCFs. The experimentally observed variation in MCF orientation within very small distances cannot be captured in 2D models as they can only represent one of the instances of this continuously varying MCF orientation within a volume. On the other hand, a 3D model represents the collective influence of the variation of MCF

orientation within a volume and captures its full effect on the mechanical response of bone at the submicroscale. In addition, 2D models cannot capture the interaction between MCFs that occur in 3D space that involve the extrafibrillar matrix.

The main limitation of the current study is the limited available experimental data on the mechanical properties of single MCFs and the extra-fibrillar matrix. In addition, there are no experimental data in the literature to validate our models. The specific submicroscale mechanical property values obtained from this study are dependent on the model assumptions related to the material properties and spatial arrangement of the MCFs and the extrafibrillar matrix. Although the predicted mechanical properties of the network may change based on the selection of the model parameters, the main findings and contribution of the study demonstrating the influence of MCF orientation, MCF size, and loading mode on the submicroscale mechanical behavior would not be affected due to the comparative nature of the study. Another point related to the model parameters is that the equivalent volume fraction of MCFs utilized in the models is not as high as some of the values reported in the literature that were in the range of 90% based on image analysis (Ascenzi and Lomovtsev, 2006). However, calculations based on weight analysis show that the equivalent MCF volume fraction is around 70% (Fritsch et al., 2009). Therefore, the values utilized in this study are in line with the weight fraction analysis, reported in the literature.

In summary, this study developed a novel modeling approach to evaluate MCF networks' mechanical response including damage and fracture behavior. The models incorporated realistic 3D MCF networks and explicit representation of extra-fibrillar matrix and evaluated both the

rupture and separation of fibrils through different modes of loading. The new framework developed in this study can generate unique information on the effect of MCF network spatial arrangement on the fracture behavior of bone at the submicroscale which is not currently possible to measure via experiments. This unique information is significant because it may improve the understanding of how the structural alterations at the submicroscale due to disease, age-related changes, and treatments affect the fracture processes at larger length scales.

**ACKNOWLEDGEMENTS**

This study was funded by National Science Foundation Award Number CMMI-1434412. The computational resources for this study were supported by XSEDE award number MSS-160001.

**CONFLICT OF INTEREST STATEMENT**

The authors have no conflict of interest to declare.

**REFERENCES**

Ascenzi, M.-G., Lomovtsev, A., 2006. Collagen orientation patterns in human secondary osteons, quantified in the radial direction by confocal microscopy. Journal of Structural Biology 153, 14-30.

Bätge, B., Winter, C., Notbobm, H., Acil, Y., Brinckmann, J., Müller, P. K., 1997. Glycosylation of human bone collagen i in relation to lysylhydroxylation and fibril diameter. The Journal of Biochemistry 122, 109-115.

Buehler, M. J., 2007. Molecular nanomechanics of nascent bone: Fibrillar toughening by mineralization. Nanotechnology 18, 295102.

Camanho, P. P., Davila, C. G., de Moura, M. F., 2003. Numerical simulation of mixed-mode progressive delamination in composite materials. J Compos Mater 37, 1415-1438.

De Falco, P., Barbieri, E., Pugno, N., Gupta, H., 2016a. Staggered fibrils and damageable interfaces lead concurrently and independently to hysteretic energy absorption and inhomogeneous strain fields in cyclically loaded antler bone. ACS Biomaterials Science & Engineering.

De Falco, P., Barbieri, E., Pugno, N. M., Gupta, H. S., 2016b. Staggered fibrils and damageable interfaces lead concurrently and independently to hysteretic energy absorption and inhomogeneous strain fields in cyclically loaded antler bone. ACS Biomaterials Science & Engineering.

Fantner, G. E., Hassenkam, T., Kindt, J. H., Weaver, J. C., Birkedal, H., Pechenik, L., Cutroni, J. A., Cidade, G. A., Stucky, G. D., Morse, D. E., Hansma, P. K., 2005. Sacrificial bonds and hidden length dissipate energy as mineralized fibrils separate during bone fracture. Nat Mater 4, 612-616.

Fantner, G. E., Schitter, G., Kindt, J. H., Ivanov, T., Ivanova, K., Patel, R., Holten-Andersen, N., Adams, J., Thurner, P. J., Rangelow, I. W., 2006. Components for high speed atomic force microscopy. Ultramicroscopy 106, 881-887.

Fratzl, P., Gupta, H., Paschalis, E., Roschger, P., 2004. Structure and mechanical quality of the collagen–mineral nano-composite in bone. Journal of materials chemistry 14, 2115-2123.

Fritsch, A., Hellmich, C., Dormieux, L., 2009. Ductile sliding between mineral crystals followed by rupture of collagen crosslinks: Experimentally supported micromechanical explanation of bone strength. Journal of Theoretical Biology 260, 230-252.

Gupta, H. S., Seto, J., Wagermaier, W., Zaslansky, P., Boesecke, P., Fratzl, P., 2006. Cooperative deformation of mineral and collagen in bone at the nanoscale. Proceedings of the National Academy of Sciences 103, 17741-17746.

Hambli, R., Barkaoui, A., 2012. Physically based 3d finite element model of a single mineralized collagen microfibril. Journal of theoretical biology 301, 28-41.

Hamed, E., Jasiuk, I., 2013. Multiscale damage and strength of lamellar bone modeled by cohesive finite elements. journal of the mechanical behavior of biomedical materials 28, 94-110.

Hang, F., Barber, A. H., 2011. Nano-mechanical properties of individual mineralized collagen fibrils from bone tissue. Journal of the Royal Society Interface 8, 500-505.

Hang, F., Gupta, H. S., Barber, A. H., 2014. Nanointerfacial strength between non-collagenous protein and collagen fibrils in antler bone. Journal of The Royal Society Interface 11, 20130993.

Hbaieb, K., Wang, Q., Chia, Y., Cotterell, B., 2007. Modelling stiffness of polymer/clay nanocomposites. Polymer 48, 901-909.

Jasiuk, I., Ostoja-Starzewski, M., 2004. Modeling of bone at a single lamella level. Biomech Model Mechanobiol 3, 67-74.

Jimenez-Palomar, I., Shipov, A., Shahar, R., Barber, A. H., 2015. Structural orientation dependent sub-lamellar bone mechanics. Journal of the Mechanical Behavior of Biomedical Materials 52, 63-71.

Kafantari, H., Kounadi, E., Fatouros, M., Milonakis, M., Tzaphlidou, M., 2000. Structural alterations in rat skin and bone collagen fibrils induced by ovariectomy. Bone 26,

349-353.

Lai, Z. B., Yan, C., 2017. Mechanical behaviour of staggered array of mineralised collagen fibrils in protein matrix: Effects of fibril dimensions and failure energy in protein matrix. Journal of the mechanical behavior of biomedical materials 65, 236-247.

Luo, Q., Nakade, R., Dong, X., Rong, Q., Wang, X., 2011. Effect of mineral–collagen interfacial behavior on the microdamage progression in bone using a probabilistic cohesive finite element model. Journal of the mechanical behavior of biomedical materials 4, 943-952.

Martin, R. B., Ishida, J., 1989. The relative effects of collagen fiber orientation, porosity, density, and mineralization on bone strength. Journal of Biomechanics 22, 419-426.

Nair, A. K., Gautieri, A., Chang, S.-W., Buehler, M. J., 2013. Molecular mechanics of mineralized collagen fibrils in bone. Nature communications 4, 1724.

Nalla, R. K., Kinney, J. H., Ritchie, R. O., 2003. Mechanistic fracture criteria for the failure of human cortical bone. Nature materials 2, 164-168.

Parry, D., Barnes, G., Craig, A., 1978. A comparison of the size distribution of collagen fibrils in connective tissues as a function of age and a possible relation between fibril size distribution and mechanical properties. Proceedings of the Royal Society of London B: Biological Sciences 203, 305-321.

Peterlik, H., Roschger, P., Klaushofer, K., Fratzl, P., 2006. Orientation dependent fracture toughness of lamellar bone. International journal of fracture 139, 395-405.

Ramasamy, J. G., Akkus, O., 2007. Local variations in the micromechanical properties of mouse femur: The involvement of collagen fiber orientation and mineralization. Journal of Biomechanics 40, 910-918.

Reilly, D. T., Burstein, A. H., 1975. The elastic and ultimate properties of compact bone tissue. J Biomech 8, 393-405.

Reznikov, N., Almany-Magal, R., Shahar, R., Weiner, S., 2013. Three-dimensional imaging of collagen fibril organization in rat circumferential lamellar bone using a dual beam electron microscope reveals ordered and disordered sub-lamellar structures. Bone 52,

676-683.

Siegmund, T., Allen, M. R., Burr, D. B., 2008. Failure of mineralized collagen fibrils: Modeling the role of collagen cross-linking. Journal of biomechanics 41, 1427-1435.

Tzaphlidou, M., 2005. The role of collagen in bone structure: An image processing approach. Micron 36, 593-601.

Tzaphlidou, M., 2008. Bone architecture: Collagen structure and calcium/phosphorus maps. Journal of biological physics 34, 39-49.

Ural, A., Vashishth, D., 2006. Interactions between microstructural and geometrical adaptation in human cortical bone. Journal of orthopaedic research 24, 1489-1498.

Wallace, J. M., Erickson, B., Les, C. M., Orr, B. G., Holl, M. M. B., 2010. Distribution of type i collagen morphologies in bone: Relation to estrogen depletion. Bone 46, 1349-1354.

Zimmermann, E. A., Schaible, E., Bale, H., Barth, H. D., Tang, S. Y., Reichert, P., Busse, B., Alliston, T., Ager, J. W., Ritchie, R. O., 2011. Age-related changes in the plasticity and toughness of human cortical bone at multiple length scales. Proceedings of the National Academy of Sciences 108, 14416-14421.

**Table 1:** Material properties of MCFs and the extra-fibrillar matrix utilized in the models. Note that $E$ is the elastic modulus, $\nu$ is the Poisson's ratio, $\sigma_{nc}$, $\sigma_{sc}$, are the normal and shear strength, respectively, and $G_c$ is the effective critical energy release rate.

| | E (GPa) | $\nu$ | $\sigma_{nc}$ (MPa) | $\sigma_{sc}$ (MPa) | $G_c$ ($Jm^{-2}$) |
|---|---|---|---|---|---|
| MCF | 2.4[a] | 0.3[b] | 120[a] | 120[c] | 1[d] |
| Extra-fibrillar matrix | - | - | 1.8[e] | 0.9[e] | 0.3[e] |

[a] (Hang and Barber, 2011)
[b] (Hambli and Barkaoui, 2012)
[c] $\sigma_{sc}$ was assigned the same value as in $\sigma_{nc}$ as there is almost no contribution of this value to damage initiation in MCFs.
[d] calculated based on the failure behavior observed in (Hang and Barber, 2011) as described in Sec. 2.1.3
[e] calculated based on values reported in (Hang et al., 2014) as described in Sec. 2.1.3.

**Table 2:** Mechanical properties of MCF networks obtained from the simulations. Note that $E$ is the elastic modulus, $\sigma_u$ is the ultimate strength, and $\gamma_a$ is the fracture energy.

| | **Diameter (nm)** | **Orientation[a]** | **E (GPa)** | **$\sigma_u$ (MPa)** | **$\gamma_a$ ($Jm^{-2}$)[b]** |
|---|---|---|---|---|---|
| **Transverse Diameter** | 60 | 0° | 0.013 | 0.309 | 0.046 |
| | 80 | 0° | 0.020 | 0.320 | 0.051 |
| | 100 | 0° | 0.024 | 0.377 | 0.062 |
| **Transverse Orientation** | 100 | ±15° | 0.015 | 0.221 | 0.040 |
| | 100 | 0°/30° | 0.025 | 0.287 | 0.049 |
| | 100 | ±30° | 0.020 | 0.244 | 0.041 |
| | 100 | ±45° | 0.042 | 0.422 | 0.063 |
| | 100 | 0°/60° | 0.060 | 0.445 | 0.075 |
| **Longitudinal Diameter** | 60 | 0° | 1.441 | 56.9 | 0.530 |
| | 80 | 0° | 1.455 | 58.6 | 0.539 |
| | 100 | 0° | 1.432 | 55.2 | 0.523 |
| **Longitudinal Orientation** | 100 | ±15° | 1.408 | 60.5 | 0.595 |
| | 100 | 0°/30° | 1.113 | 45.3 | 0.578 |
| | 100 | ±30° | 1.103 | 46.9 | 0.575 |
| | 100 | ±45° | 0.857 | 34.4 | 0.411 |
| | 100 | 0°/60° | 0.672 | 25.5 | 0.259 |
| | 100 | 0°/90° | 0.419 | 16.3 | 0.203 |

[a] All orientation values incorporate a dispersion value of ±15° as outlined in Sections 2.1.1 and 2.3.
[b] Fracture energy was evaluated at a strain of $\varepsilon = 0.05$ for longitudinal and $\varepsilon = 0.3$ for transverse models as outlined in Section 2.4.

**FIGURE CAPTIONS**

**Figure 1:** Steps of MCF network generation. Separate groups of (a) long and (b) short MCFs (c) Non-overlapping long MCF groups (d) Trimming of overlapping MCFs (e) Assembled MCF network model consisting of trimmed long and short fibrils.

**Figure 2:** Schematics of the loading and boundary conditions of the models under (a) longitudinal and (b) transverse loading with respect to the main MCF orientation.

**Figure 3:** Traction ($T$) – crack separation ($\delta$) relationship defined by ultimate strength ($\sigma_c$) and critical energy release rate ($G_c$). $\delta u$ is the ultimate crack separation distance. The initial ascending dotted line represents the elastic response of the material and is defined as a penalty stiffness (Camanho et al., 2003) and only applies for cohesive interface elements but not required for the XFEM formulation.

**Figure 4:** Undeformed (1$^{st}$ column) and deformed shapes including damage and crack formation under transverse (2$^{nd}$ column) and longitudinal (3$^{rd}$ column) loading for (a) Orientation: 0°, Diameter: 60±5nm; (b) Orientation: 0°, Diameter: 100±5nm; (c) Orientation: ±30°, Diameter: 100±5nm; (d) Orientation: 0°/60°, Diameter: 100±5nm. The colors represent the damage accumulation in a rainbow contour where red is full crack and dark blue is the lowest damage.

**Figure 5:** Influence of MCF diameter on stress-strain relationship under (a) longitudinal and (b) transverse loading.

**Figure 6:** Influence of MCF orientation on stress-strain relationship under (a) longitudinal and (b) transverse loading. Note that the simulation for 0°/90° is the same for both longitudinal and transverse loading, therefore, the result of that model is only shown in (a).

**Figure 1**

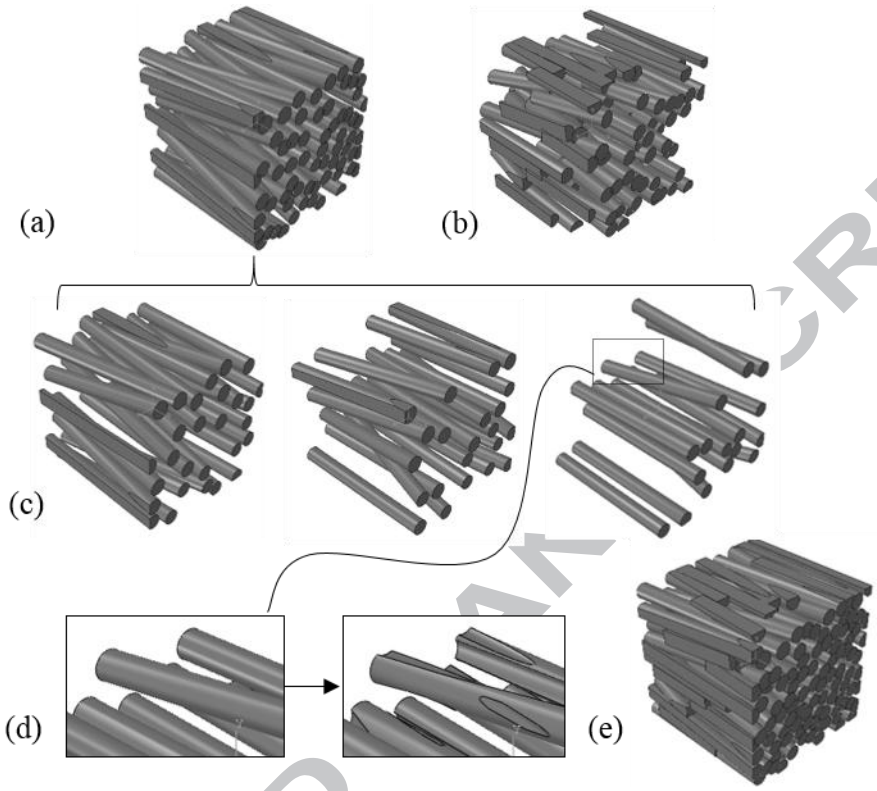

**Figure 2**

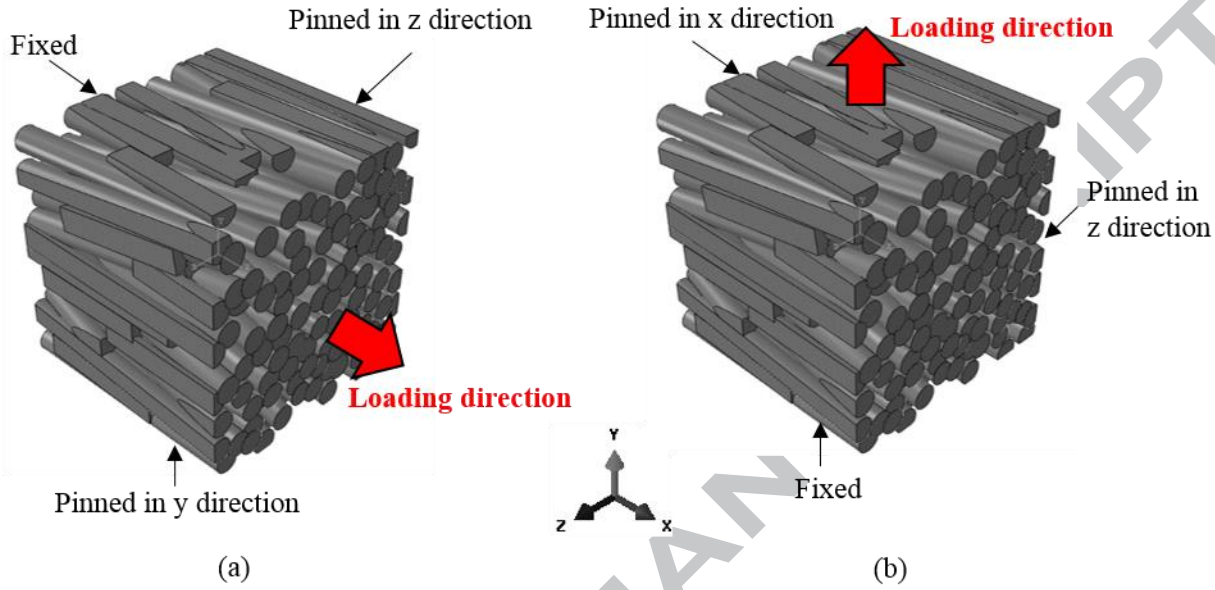

**Figure 3**

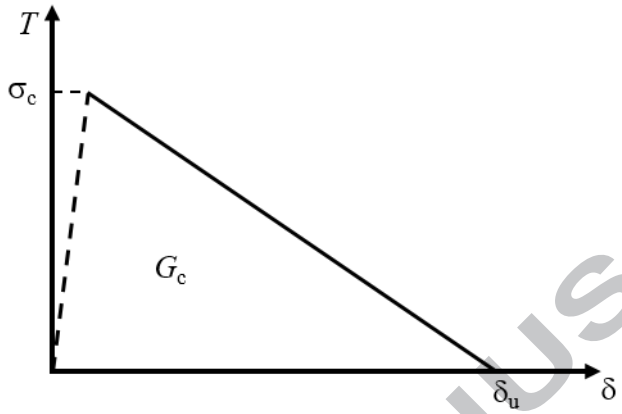

**Figure 4**

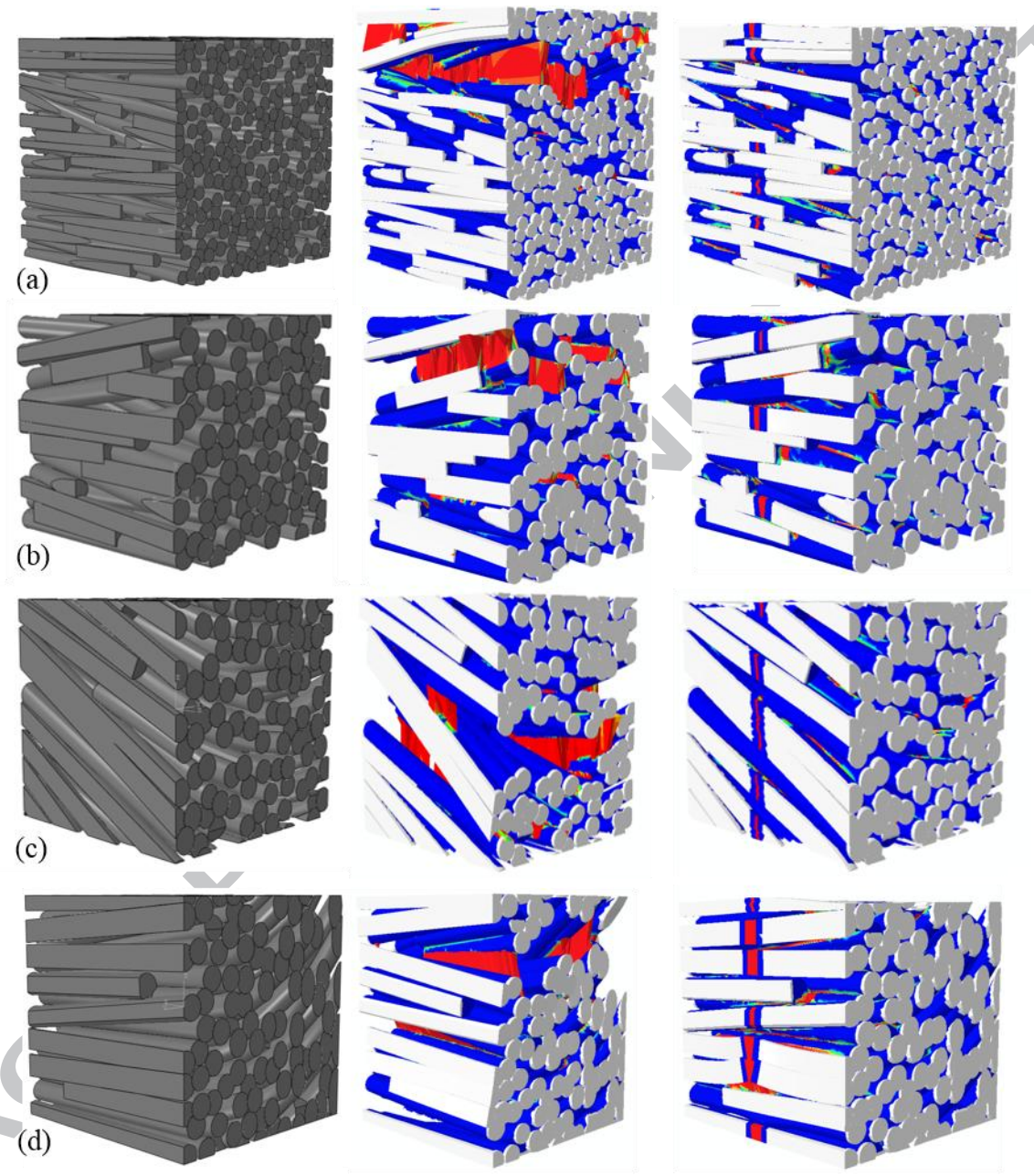


**Figure 5**

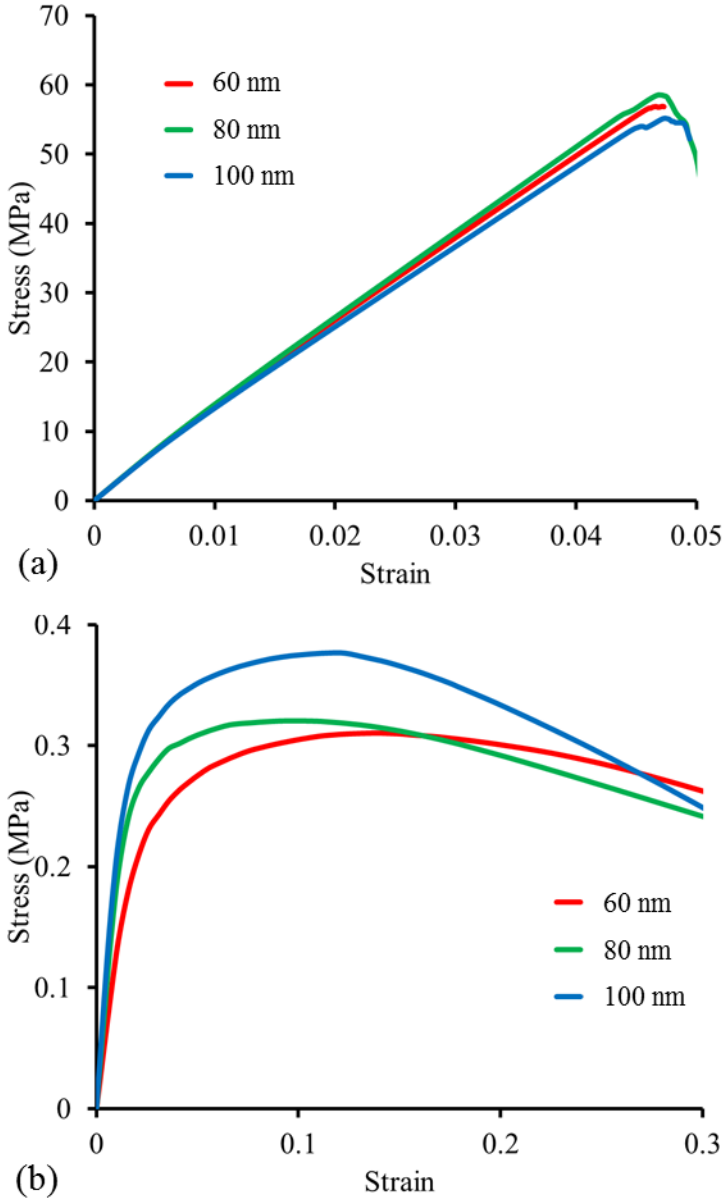

**Figure 6**